INSTITUTE OF PHYSICS PUBLISHING WAVES IN RANDOM MEDIA

Waves Random Media **14** (2004) S7–S27 PII: S0959-7174(04)68768-4

Form factor for large quantum graphs: evaluating orbits with time reversal

Gregory Berkolaiko

Department of Mathematics, University of Strathclyde, Glasgow G1 1XH, UK

Received 19 March 2003
Published 5 December 2003
Online at stacks.iop.org/WRM/14/S7 (DOI: 10.1088/0959-7174/14/1/008)

Abstract

It has been shown that for a certain special type of quantum graphs the random-matrix form factor can be recovered to at least third order in the scaled time τ using periodic-orbit theory. Two types of contributing pairs of orbits were identified: those which require time-reversal symmetry and those which do not. We present a new technique of dealing with contributions from the former type of orbits.

The technique allows us to derive the third-order term of the expansion for general graphs. Although the derivation is rather technical, the advantages of the technique are obvious: it makes the derivation tractable, it identifies explicitly the orbit configurations which give the correct contribution and it is more algorithmic and more system-independent, making possible future applications of the technique to systems other than quantum graphs.

(Some figures in this article are in colour only in the electronic version)

1. Introduction

The Bohigas–Giannoni–Schmit conjecture [1] asserts that the spectral correlations in quantum systems with chaotic classical analogues fall into several universality classes, depending on the symmetries of the system. In particular, the spectral correlations of systems with time-reversal (TR) symmetry coincide with the relevant expressions obtained in random matrix theory for orthogonal ensembles of matrices. This claim was supported by a multitude of numerical examples [2], but for a long time the only theoretical advance for individual systems (i.e. without a disorder average) was Berry's diagonal approximation [3]. The recent work of Sieber and Richter [4] and Sieber [5] has renewed the hope that the universality of spectral correlations can be explained within periodic-orbit (PO) theory.

One of the more convenient statistics is the Fourier transform of the spectral two-point correlator, the form factor, whose universal expression for orthogonal ensembles is given by the formula [6]

$$K_{\mathrm{GOE}}(\tau) = 2\tau - \tau\log(1+2\tau) = 2\tau - 2\tau^2 + 2\tau^3 + \mathrm{O}(\tau^4), \tag{1}$$

 © 2004 IOP Publishing Ltd Printed in the UK

when τ is in the range $0 \leqslant \tau \leqslant 1$. For a quantum chaotic system the form factor can be written in terms of a double sum over POs using the Gutzwiller trace formula [7]. This double sum is the usual starting point for analysis, in which different classes of PO pairs are identified and their contribution is evaluated to reproduce the small-τ expansion of the prediction (1).

Berry [3] calculated the leading contribution to the form factor by neglecting all correlations between POs other than exact symmetries. Within this 'diagonal approximation', he obtained the leading order term in the τ expansion. In [4, 5] it was shown, that for uniformly hyperbolic and TR invariant billiards on surfaces with constant negative curvature the second-order contribution $-2\tau^2$ is related to correlations within pairs of orbits differing in the orientation of one of the two loops resulting from a self-intersection of the orbit. The same result, but without the restriction to uniformly hyperbolic dynamics, was derived for a large family of quantum graphs [10]. In particular, some progress has been made in identifying the exact requirements of the degree of 'chaoticity' of the graphs. The further step to third order was performed in [11], where some of the classes of orbits were evaluated for general graphs. However, for classes of orbits which explicitly required TR symmetry, the uniform hyperbolicity had to be assumed. At this time it became clear that the method used in [10] would become intractable for the third order in general graphs and deriving the fourth-order term would be quite impossible, even for systems with uniformly hyperbolic dynamics.

The present paper presents a different method of dealing with various classes of orbits. The underlying idea is the repeated application of the inclusion–exclusion principle to obtain a decomposition of orbit pairs into sets of which only a relatively small proportion give a nonzero contribution. This technique has several advantages: the derivation becomes tractable for general graphs, the orbit classes giving the universal contributions are identified explicitly and the application of the technique is a relatively mechanical process which decreases the chance of missing a contribution and raises the hope of a general derivation of the expansion to all orders. It is also worth mentioning that the technique is relatively system-independent in that it does not use any features specific to quantum graphs, operating on rather abstract *diagrams*.

This paper is organized as follows: in section 2 we define our model and explain how the form factor can be expressed as a double sum over POs. In section 3 this sum is rewritten in terms of diagrams, representing all orbits with a given number and topology of self-intersections. Diagrams contributing to the first three orders are identified. In section 4 we explain our method by re-deriving the second-order contribution and then proceed to apply it to obtain the third-order term.

2. Quantum graphs and periodic-orbit theory

We consider graphs with N vertices connected by B directed bonds. A bond leading from vertex m to vertex l is denoted by (m, l). Since we are considering graphs with TR invariance, it is necessary that for any bond (m, l) there exists also the reversed bond (l, m). We do not rule out the possibility of loops, i.e. bonds of the form (m, m), which are TR-invariant.

The discrete quantum dynamics on a graph is defined in terms of a $B \times B$ unitary time-evolution operator $S^{(B)}$ with matrix elements

$$S^{(B)}_{m'l',lm} = \delta_{l'l}\, \sigma^{(l)}_{m'm} \mathrm{e}^{\mathrm{i}\phi_{ml}} \tag{2}$$

describing the transition amplitudes from the directed bond (m, l) to (l', m'). Here the Kronecker delta ensures that a transition is possible only between joined bonds and $\sigma^{(l)}_{m'm}$ denotes the *vertex-scattering matrix* at vertex l. The phases ϕ_{ml} are random variables distributed uniformly in $[0, 2\pi]$ and, for a fixed B, they define an ensemble of matrices $S^{(B)}$ which is used

below for averaging. The form factor is defined at integer times $t = 0, 1, \ldots$ by

$$K^{(B)}(\tau) = B^{-1}\langle |\operatorname{tr} S^{\mathrm{t}}|^2\rangle_{\{\phi\}}, \tag{3}$$

where τ is the scaled time $\tau = t/B$ and $\langle\cdots\rangle$ denotes the averaging. We are interested in the limit of large graphs $B \to \infty$, keeping the scaled time τ fixed:

$$K(\tau) = \lim_{B\to\infty} K^{(B)}(\tau), \tag{4}$$

since this is equivalent to the semiclassical limit of chaotic systems [8, 9]. It is in this limit that the form factor is expected to assume the corresponding universal form (1).

The classical analogue of the quantum graph [8, 9, 12] is represented by a Markov chain on the graph, specified by the doubly stochastic matrix M of transition probabilities:

$$M_{m'l,lm} = |S^{(B)}_{m'l,lm}|^2 = |\sigma^{(l)}_{m'm}|^2. \tag{5}$$

Matrix elements of powers of M give the classical probability to get from bond (m, l) to bond (k, n) in t steps:

$$P^{(t)}_{(m,l)\to(k,n)} = [M^{\mathrm{t}}]_{nk,lm}. \tag{6}$$

Under very general assumptions it can be shown that the dynamics generated by M is ergodic and mixing [13], i.e. for fixed B and $t \to \infty$ all transition probabilities become equal:

$$P^{(t)}_{(m,l)\to(k,n)} \to B^{-1} \qquad \text{as } t \to \infty \quad \forall (m, l), (k, n). \tag{7}$$

However, since in (4) the limits $B \to \infty$ and $t \to \infty$ are connected by fixing τ, we need a stronger condition such as

$$P^{(\tau B)}_{(m,l)\to(k,n)} \to B^{-1} \qquad \text{as } B \to \infty \quad \forall (m, l), (k, n). \tag{8}$$

The requirements on the speed of convergence depend on the order to which agreement with (1) is required. To avoid unpleasant estimates we will restrict ourselves to graphs for which the convergence is faster than any power of B.

Another, somewhat related, condition is that the probability of following a self-retracing orbit of length $O(B)$ is negligible. More rigorously, define a matrix R by squaring the elements of the matrix M:

$$R_{m'l,lm} = |S^{(B)}_{m'l,lm}|^4 = |\sigma^{(l)}_{m'm}|^4. \tag{9}$$

We require that for any γ

$$\sum_{n,k,l,m} [R^{\gamma B}]_{nk,lm} \to 0 \qquad \text{as } B \to \infty \tag{10}$$

faster than any power of B.

The above conditions are in agreement with what is known about various special classes of graphs. The conditions are satisfied, for example, by complete graphs with either Neumann or Fourier vertices [11] where numerical evidence strongly supports the BGS conjecture [9, 14] and are not satisfied by graphs with Dirichlet vertices and Neumann star graphs [15], which are known to produce non-RMT statistics.

A connection between the quantum form factor (3) and the classical dynamics given by (5) can be established by representing the form factor as a sum over (classical) POs. A PO is a sequence of vertices $P = [p_1, \ldots, p_t]$ defined up to a cyclic shift and such that (p_i, p_{i+1}) is a bond of the graph for every $i = 1, \ldots, t$.

By expanding the matrix powers of S in (3) and averaging over phases ϕ one arrives at the PO expansion of the form factor [9, 11]

$$K^{(B)}_{\mathrm{TR}}(\tau) = \frac{t^2}{B}\sum_{P,Q} A_P A^*_Q, \tag{11}$$

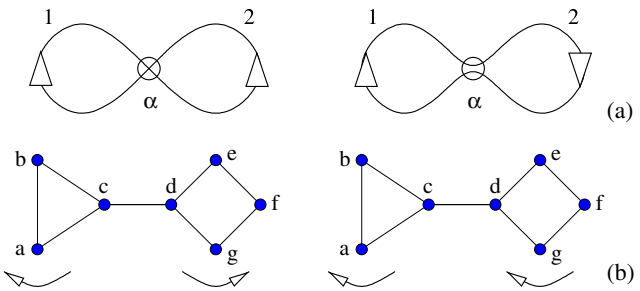

Figure 1. A schematic representation of an orbit with a self-intersection at a vertex α and its partner orbit (a). There are orbits, however, for which the position of the intersection point α is ambiguous. The pair of orbits shown in (b) can be fitted into the pattern (a) with either c or d playing the role of the intersection vertex.

where A_P is the product of σ matrices along the orbit P: $A_P = \sigma^{(p_2)}_{p_1 p_3}\sigma^{(p_3)}_{p_2 p_4}\cdots\sigma^{(p_1)}_{p_n p_2}$, the star denotes the complex conjugation and, most importantly, the sum is taken over only those pairs of orbits that visit *the same set of bonds, or their time-reversed equivalents, the same number of times*.

3. The expansion in self-intersections of the periodic orbits

3.1. From orbits to diagrams

The calculation of the form factor is now reduced to a combinatorial problem: ensure that P and Q pass through the same non-directed bonds. This can be done by composing P and Q from the same segments, or *arcs*, which would appear in P and Q in different order and/or orientation. We classify the pairs of orbits in the following manner. We fix a *transformation*: a permutation of arcs followed by the TR of selected arcs and then sum over all orbits P, Q related by this transformation. The clearest way to represent a transformation is graphical, hence we refer to them as *diagrams*. The sum over all diagrams finally gives the form factor.

The main problem with this approach is to ensure that each orbit pair P, Q is counted once and only once. This is difficult because for a given pair P, Q the identification of the arcs and their permutation, transforming P into Q, is not necessarily unique. As a simple example consider the diagrams in figure 1. Part (a) gives a schematic representation of the pair P, Q, where Q is obtained from P by reversal of arc 2. Such orbits were considered in [10] and were shown to give the contribution $-2\tau^2$. One of the difficult points of the derivation was correctly counting the orbits which do not merely cross but follow themselves for at least one bond. An example of such an orbit is given in part (b), where the orbit crosses itself along the bond (c, d). For such an orbit, there are two possibilities to identify arc 1: either as $\to a \to b \to$ or as $\to c \to a \to b \to c \to$, thus taking either c or d as the intersection point.

To avoid this double-counting, [10] imposed a *restriction* on arc 1. Denoting the first vertex of the arc by s_1 and the last one by f_1, it was demanded that $s_1 \neq f_1$. This ensured the unique choice of the arcs and the intersection point. In the example above, the valid choice is $\to a \to b \to$.

Unfortunately, even with this restriction, there were orbits that should not be counted: those *exceptions* had self-retracing arc 2. The self-retracing arc did not change under TR and, as a result, the orbit Q was identical to the orbit P, forming a pair which was already counted in the diagonal approximation. The contribution of such orbits had to be subtracted explicitly.

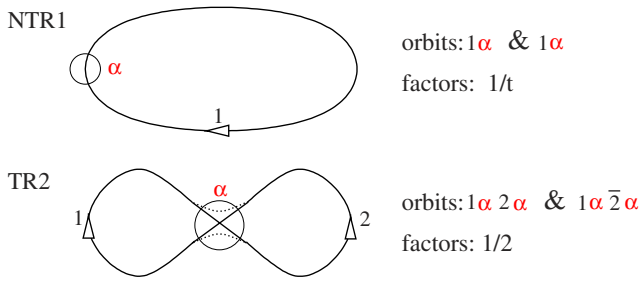

Figure 2. Topology of orbits contributing to the form factor at first and second orders. Evaluating the NTR1 orbits we recover the diagonal approximation to the form factor.

In this paper we present a different counting technique, which is easily extendable to more complicated diagrams, avoids the introduction of exceptions and explicitly identifies the orbits which give the generic contribution. We will first illustrate our approach by re-deriving the $-2\tau^2$ contribution and then proceed to calculate the third-order correction. But before we can do it, we need to introduce the notation and discuss some preliminary matters.

3.2. Notation

If we consider P as a single arc with no intersections, $Q = P$ and $\bar{P}$ are the only options. Here the bar denotes the operation of TR. The corresponding diagram has a simple circular shape (the first diagram of figure 2). Summation over these orbit pairs is nothing other than the diagonal approximation. It produces $K_1 = 2\tau$. In [10] orbit P was treated as two arcs, 1 and 2, joined at a single intersection α, corresponding to an figure-eight-shaped diagram, figure 2. The contributions of such orbits were found to give rise to the second-order term in (1), $K_2 = -2\tau^2$. In this paper we calculate the τ^3 contribution by assuming that P contains three or four arcs connected at intersections.

We denote arcs by numbers $1, 2, \ldots$ and the intersection points by Greek letters $\alpha, \beta, \ldots$. An arc can be identified by a sequence of vertices, which does not include the intersection vertices, or, alternatively, by a sequence of bonds, which includes the bonds from and to the intersection points. The length of the ith arc is denoted by t_i and is defined as the number of bonds in the arc (which is one more than the number of vertices in the arc). The sum of the lengths of all arcs gives t, the length of the orbit. The length of an arc is at least one. Given an arc i leading from α to β we denote the first vertex following α by s_i and the last vertex before β by f_i. In the degenerate case when the arc going from α to β is the single bond (α, β) and does not contain any vertices ($t_i = 1$) our definition implies $s_i = \beta$ and $f_i = \alpha$.

The diagrams contributing at the third order are shown in figure 3. For a discussion of why only these particular diagrams contribute at third order in τ we refer the reader to [11]. In any diagram, the arcs forming the orbit P and its partner Q are identical, but the way they are connected at the intersections differs. The orbit P is given by the connections drawn as continuous lines, while its partner orbit Q is given by connections drawn as dotted lines. The orbits P and Q are also written as a symbolic code to the right of each diagram: a path that goes from the beginning of arc 1 to vertex α then on arc 2 to vertex β and so on is denoted as $1\alpha 2\beta \ldots$. The diagrams divide into two classes, NTR and TR. In the NTR diagrams all the arcs of Q have the same orientation as the corresponding arcs in P, while in the TR diagrams some of the arcs of Q are time-reversed. For a system with no TR symmetry, only the NTR diagrams are possible. In our case, diagrams in both classes contribute and τ^3 contributions to the form factor is a sum of five terms:

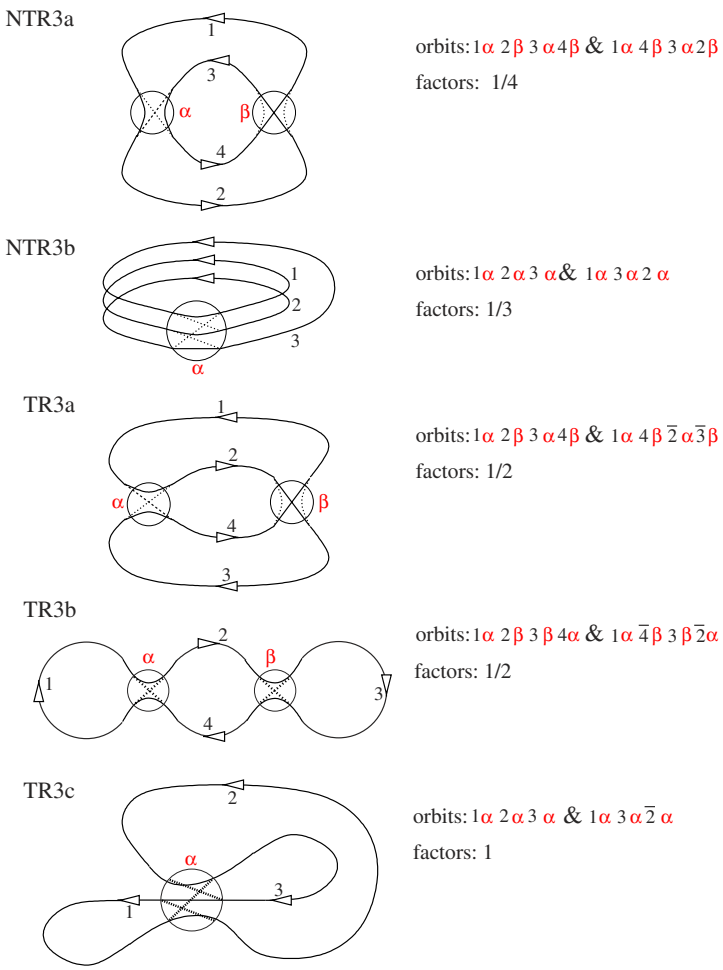

Figure 3. Topology of NTR3a, NTR3b, TR3a, TR3b and TR3c. In each case a pair of orbits is shown: one follows the full curve throughout, while the second follows the full curve except at the intersections (denoted by circles) where it follows the dotted line. Each circle represents a single vertex where a self-intersection of the orbit occurs. Next to each topology we give the symbolic code for the pair and the corresponding weight factor (section 3.3).

$$K_3 = 2(K_{\mathrm{NTR3a}} + K_{\mathrm{NTR3b}} + K_{\mathrm{TR3a}} + K_{\mathrm{TR3b}} + K_{\mathrm{TR3c}}). \tag{12}$$

The factor of 2 is due to the fact that, for every diagram in figure 3, there is another one with Q replaced by its complete TR, $\bar{Q}$, which gives an identical contribution.

The NTR diagrams were treated in the general case in [11] and it was shown that $K_{\mathrm{NTR3a}} + K_{\mathrm{NTR3b}} = 0$. In this paper we derive the contribution of TR diagrams using a slightly different method.

3.3. Avoiding double-counting

There are degeneracies in the diagrams which can be accounted for by simple prefactors multiplying the contributions such as the factor of two in (12). These factors were derived in [11] and are listed in figure 3 next to the diagrams.

Another potential source for double-counting of orbits are *tangential* intersections, already mentioned in section 3.1. Double-counting can be avoided using a method outlined in [10] and followed in [11]: the intersection point is uniquely defined by ruling that if there is an ambiguity then the intersection is as far to one side as possible. As an example we refer to the ambiguous intersections in figure 1(b) and insist the intersection is as far to the left as possible. That is, we demand that the vertices a and b are distinct.

Contrary to what was done in [11], we will not fix the restrictions for the TR diagrams. The restrictions we choose will depend on the lengths of individual arcs, as will be shown in section 4.

It should be emphasized that the orbits with tangential self-intersections are responsible for non-zero contributions to the form factor and their correct treatment is absolutely crucial to the derivation.

3.4. Orbit amplitudes

Before we can attempt the summation over all orbit pairs P, Q within a given diagram, we need to understand the structure of the product $A_P A_Q^*$ appearing in (11). We consider the diagram TR2 as an example. Let arc 1 be of length t_1, consisting of the vertices $[s_1, x_2, x_3, \ldots, x_{t_1-2}, f_1]$. Then both A_P and A_Q will contain factors $\sigma^{(s_1)}_{x_2\alpha}, \sigma^{(x_2)}_{x_3x_1}, \sigma^{(x_3)}_{x_4x_2} \cdots \sigma^{(x_{t_1-2})}_{\alpha x_{t_1-3}}$. Thus when we evaluate the product $A_P A_Q^*$, the contribution of arc 1 will come in the form

$$|\sigma^{(x_1)}_{x_2\alpha}\sigma^{(x_2)}_{x_3x_1}\sigma^{(x_3)}_{x_4x_2}\cdots\sigma^{(x_{t_1-2})}_{\alpha x_{t_1-3}}|^2 = P_{(\alpha,x_1)\to(x_1,x_2)\to(x_2,x_3)\to\cdots\to(f_1,\alpha)} \equiv P_1, \tag{13}$$

which is the classical probability of following arc 1 from bond (α, s_1) to bond (f_1, α)[1]. Analogous construction leads to the probability P_2 of following arc 2: here we need to remember that the matrices σ are symmetric. The factors not yet accounted for in P_1 and P_2 are the transition amplitudes picked up at the intersection vertex α:

$$A_P A_Q^* = P_1 \times P_2 \times \sigma^{(\alpha)}_{f_2s_1}\sigma^{(\alpha)}_{f_1s_2} \times \left(\sigma^{(\alpha)}_{s_2s_1}\sigma^{(\alpha)}_{f_1f_2}\right)^*. \tag{14}$$

To evaluate the contribution of the diagram, (14) must be summed over all free parameters, namely all intersection points and all possible arcs connecting these points. The latter summation includes a sum over the lengths t_i of these arcs, with the restriction that the total length of the orbit is t.

The summation over all the intermediate vertices $x_2, x_3, \ldots, x_{t_1-2}$ along arc 1 can be performed immediately, since it is unaffected by the restrictions discussed in the previous subsection. This summation adds the classical probabilities of all possible paths leading from bond (α, s_1) to bond (f_1, α) in $t_1 - 1$ steps and results in the classical transition probability $P^{(t_1-1)}_{(\alpha,s_1)\to(f_1,\alpha)}$ given by (6). Analogous summation over the other arc produces $P^{(t_2-1)}_{(\alpha,s_2)\to(f_2,\alpha)}$.

The remaining summation is over the lengths t_i of all arcs, the first and the last vertex s_i and f_i of all arcs i with $t_i > 1$ and the intersection points like α. Here we try to use the fact that for sufficiently long arcs the transition probabilities can be replaced by B^{-1} according to (8). Then the sum over vertices decouples into a product of sums associated with the intersection vertices, which can finally be evaluated using the unitarity of the vertex-scattering matrices σ.

[1] $P_1 = 1$ if arc 1 contains no vertices, i.e. if $t_1 = 1$.

4. Summation of TR diagrams

4.1. TR2

As was mentioned earlier, we develop a slightly different technique to deal with the TR diagrams. We will illustrate it by first considering the TR2 contribution. In [10] we dealt with the intersection point ambiguity by imposing a restriction $s_2 \neq f_2$. The summation would then take the form

$$K_{\mathrm{TR2}}(\tau) = \frac{1}{2}\frac{t^2}{B}\sum_{\{t_i\}}\delta\Big[t - \sum_{i=1}^{2} t_i\Big]\sum_{\alpha}\sum_{\{s_i,f_i\}}\Sigma_{\mathrm{TR2}}\times P_{\mathrm{TR2}}\times\Delta_{\mathrm{TR2}}, \tag{15}$$

where

$$\Sigma_{\mathrm{TR2}} = \sigma^{\alpha}_{f_2 s_1}\sigma^{\alpha}_{f_1 s_2}\sigma^{\alpha *}_{s_2 s_1}\sigma^{\alpha *}_{f_1 f_2} \tag{16}$$

$$P_{\mathrm{TR2}} = P^{t_1-1}_{(\alpha,s_1)\to(f_1,\alpha)}P^{t_2-1}_{(\alpha,s_2)\to(f_2,\alpha)} \tag{17}$$

$$\Delta_{\mathrm{TR2}} = (1-\delta_{s_2 f_2}). \tag{18}$$

Since at least one of the arcs must be long, we can approximate the corresponding $P^{t_i-1}_{(\alpha,s_i)\to(f_i,\alpha)}$ by its ergodic limit $1/B$. If arc 1 is long, we can perform the summation over s_1 (or f_1):

$$(1-\delta_{s_2 f_2})\sum_{s_1}\sigma^{\alpha}_{f_2 s_1}\sigma^{\alpha *}_{s_2 s_1} = (1-\delta_{s_2 f_2})\delta_{s_2 f_2} \equiv 0 \tag{19}$$

to show that the contribution of such orbits is zero. However, the case when arc 2 is long is not nearly as easy. We can still sum over s_2 or f_2, but the restriction, which helped us in the first part, now stands in the way (see [10] for details).

The idea that we are going to use is as follows: we can change the restrictions depending on the arc lengths. In the TR2 case, if arc 1 is long, we stick with the restriction $s_2 \neq f_2$, and if arc 2 is long, we switch to the restriction $s_1 \neq f_1$. In the first case the result of the summation is 0, as was shown above. In the second case we approximate $P^{t_2-1}_{(\alpha,s_2)\to(f_2,\alpha)}$ by $1/B$ and perform the summation over s_2 to obtain

$$(1-\delta_{s_1 f_1})\sum_{s_1}\sigma^{\alpha}_{f_1 s_2}\sigma^{\alpha *}_{s_2 s_1} = (1-\delta_{s_1 f_1})\delta_{s_1 f_1} \equiv 0. \tag{20}$$

This is not what we should be getting: the overall result should be $-2\tau^2$, not 0. The reason for getting 0 is that there are orbits which were counted in both sums. To explain this, we need to define more carefully what is meant by 'arc i is long'.

We split the set of all TR2 orbit pairs into two sets. The set A will contain orbits satisfying $t_1 \geqslant t/2$ and $s_2 \neq f_2$. The set B will contain orbits satisfying $t_1 < t/2$ and $s_1 \neq f_1$. The sum of contributions coming from each set is zero, as was shown in the previous paragraph. However, these sets are not disjoint. Figure 4 illustrates both sets, denoted by A and B, and the shape of the orbits belonging to their intersection $A \cap B$. These are orbits with a tangential intersection which is roughly in the middle of them: $t_1 < t/2$ but $t_1 + 2a \geqslant t/2$, where a is the length of the intersection and t_1 is now counted from the end of the tangential intersection (i.e. from vertex α_0). We need to subtract the contribution of such orbits to recover the full term $K_{\mathrm{TR2}}(\tau)$.

To calculate the contribution of the orbits in $A \cap B$, we notice (see the appendix) that we get the same contribution if we modify the set $A \cap B$ by setting $a = 1$ and dropping the constraints. Thus we can write for this contribution

$$|A \cap B| = \frac{t^2}{2B}\sum_{t_1,t_2}\sum_{\alpha_0,\alpha_1}P^{t_1+1}_{(\alpha_1,\alpha_0)\to(\alpha_0,\alpha_1)}P^{t_2+1}_{(\alpha_0,\alpha_1)\to(\alpha_1,\alpha_0)} \tag{21}$$

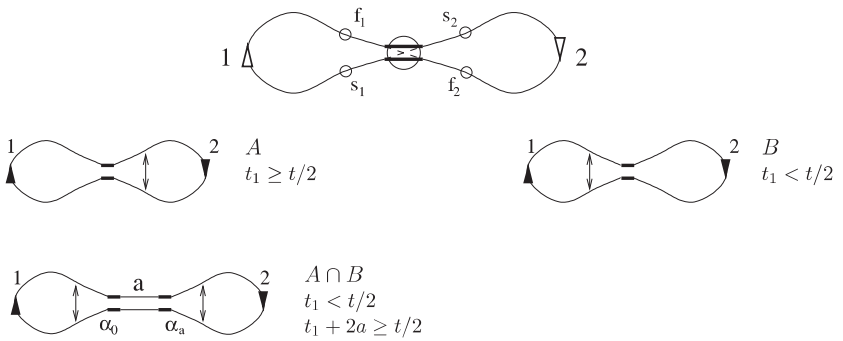

Figure 4. The TR2 diagram and its partition into two sets of orbits. The total contribution of the orbits in each set is easily shown to be zero. The result comes from the orbits lying in the intersection of the two sets, $A \cap B$.

where $t = t_1 + t_2 + 2$ and, because of the tangential intersection, the unitary factors at the intersection point were squared and absorbed into the classical probability. In fact, the whole expression is purely classical now. The length of arc 1 must satisfy $t_1 < t/2$ and $t_1 + 2 \geqslant t/2$. Thus there are only two possible values that t_1 can take: $t/2 - 1$ and $t/2 - 2$. The length of arc 2 satisfies $t_2 = t - 2 - t_1$ and therefore both arcs are long and the corresponding probabilities can be approximated by $1/B$:

$$|A \cap B| = \frac{t^2}{2B^3} \sum_{t_1,t_2} \sum_{\alpha_0,\alpha_1} 1 = \frac{t^2}{2B^3} 2 \sum_{\alpha_0,\alpha_1} 1 = \frac{t^2}{B^2} \to \tau^2, \tag{22}$$

where the last sum is taken over all *connected* pairs of vertices α_0 and α_1 and the factor of 2 appeared because there are only two possible choices of the lengths $\{t_1, t_2\}$. To get the final result for $K_{\mathrm{TR2}}(\tau)$, we need to multiply (22) by two once more, to account for the TR symmetry, and subtract it from the previous result (zero) since these orbits were double-counted when we calculated the contributions of the sets A and B. Hence we obtain the sought-after result $K_{\mathrm{TR2}}(\tau) = -2\tau^2$. It is important to note that in the above derivation we could have used any $\mathrm{O}(t)$ value instead of $t/2$.

Now our strategy of dealing with the diagrams of higher order is clear. We will strive to partition the orbits belonging to each diagram into several sets, such that the contribution of each set is easily seen to be zero. The intersections of these set will provide the true contributions to the form factor. Hopefully, the arcs of the orbits in the intersections will be long and thus the ergodic approximation can be employed to simplify the calculations.

4.2. Partition of TR3a

Before we start making partitions of the diagrams, we stress that there is no unique 'right' way to partition. The partition that we are presenting here is only one of those that we considered. All partitions produce the same results, as they should, but the present one seemed to be the least difficult.

The suggested partition for the diagram TR3a is given by figure 5 (upper part). Each of the four subsets of TR3a is equipped with its own set of constraints, which are shown by the arrows. For example, the set A has constraints $f_1 \neq f_3$ and $s_3 \neq f_4$. The constraints are chosen in such a way that the contributions of each set evaluate to zero: for example, the arc 1 is long in the set A, so we can approximate the contribution of the arc by its ergodic limit and subsequently sum over s_1 to obtain zero. The constraints also take into account the symmetry of the diagram: under the permutation of arcs $1 \leftrightarrow 3$ and $2 \leftrightarrow 4$, the set A is interchanged

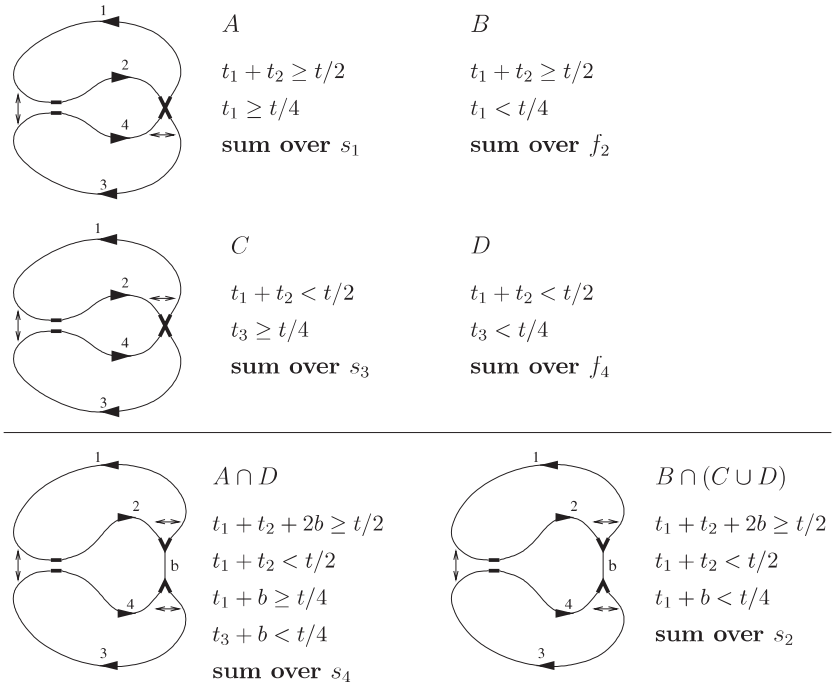

Figure 5. The TR3a diagram and its partition into four sets of orbits. The orbits of the sets A and B have identical structure but different lengths. The same applies to the sets C and D. A consequence of this is that $A \cap B = C \cap D = \emptyset$, which implies that all three-way intersections are empty. The contribution of the orbits in each set can be easily shown to be zero. Also drawn in the figure are three of the four two-way intersections among the partition sets of the TR3a diagram. The contribution of each is zero.

with C and B is interchanged with D. Also, it is immediately obvious that the sets A and B are disjoint; so are the sets C and D. Therefore we do not have to worry about three-way intersections of the partition sets.

Three of the two-way intersections are straightforward to evaluate, see figure 5. The intersection $A \cap D$ has $t_1 + t_2 \approx t/2$ and therefore $t_3 + t_4 \approx t/2$ but $t_3 + b < t/4$. Therefore the arc 4 is long and we can sum over s_4, obtaining zero. The intersections $B \cap C$ and $B \cap D$ can be considered together, as $B \cap (C \cup D)$. For this set we again have $t_1 + t_2 \approx t/2$ and t_1 is small, thus enabling us to sum over s_2.

The last intersection, $A \cap C \equiv E$, is the hardest, see figure 6. Arcs 2 and 4 are potentially short and summation over any other arc is obstructed by the constraints. To overcome this, we change the constraint $f_1 \neq f_3$ to $s_2 \neq s_4$, thus producing the set E_1. There are certain orbits, however, that belong to E and do not belong to E_1 and vice versa. These are put into the sets E_2 and E_3, correspondingly. The orbits from the set E_1 can be easily shown to produce zero contribution. The contribution of the sets E_2 and E_3 are not zero and will be evaluated separately.

4.3. Partition of TR3b

Diagram TR3b is split into three sets, figure 7. Here r is a large number, of order $t/4$. The reason we do not just put it equal to $t/4$ is to highlight the interaction of diagram TR3b with TR3c.

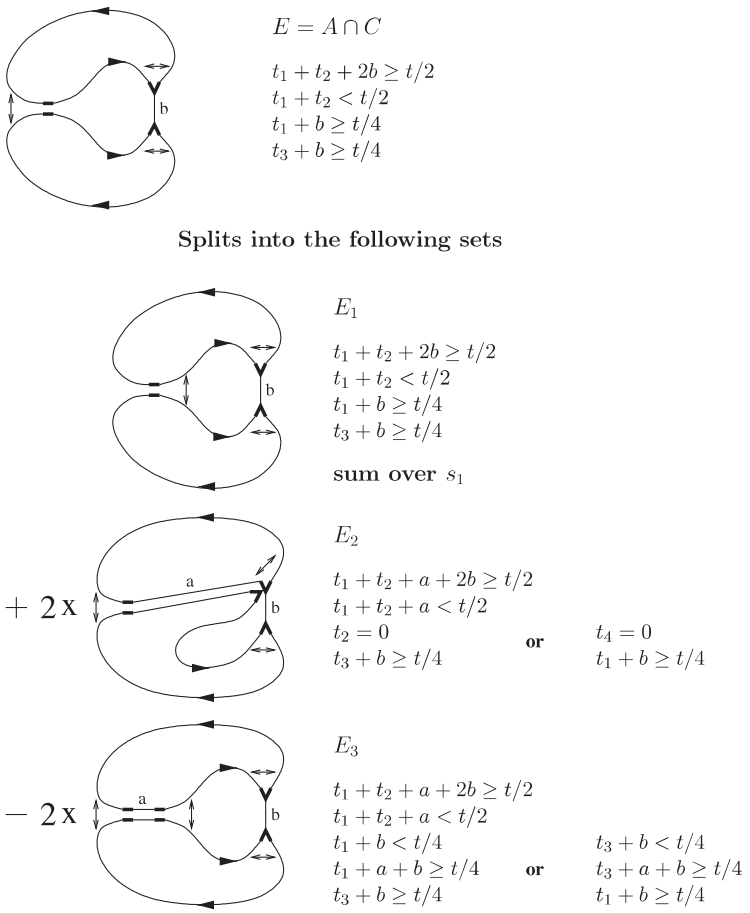

Figure 6. The last of the two-way intersections among the partition sets of the TR3a diagram. To evaluate it we represent it as the set E_1 plus the orbits in the set E_2 minus the orbits of the set E_3. The contribution of the set E_1 is zero.

To show that the contribution of the sets A and B is zero, simply sum over s_1 and s_3 correspondingly. In set C, at least one of arcs 2 and 4 is long, thus enabling us to sum over s_2 or s_4. It is easy to see that the sets A and B are disjoint.

The intersection $A \cap C$ is also shown in figure 7. One of arcs 2 and 4 must be long. To be able to sum, we need to drop the restriction $f_2 \neq s_4$, producing the set F_1. By summing either over f_2 or s_4 (depending on which arc is longer), we show that the contribution of F_1 is zero. However, the set F_1 is larger than $A \cap C$: it includes the orbits sketched in the sets F_2, those can be obtained if, say, arc 4 is one bond long and $f_2 = s_4$. The set F_2 provides a non-zero contribution and will be evaluated separately.

In a similar fashion we treat the intersection $B \cap C$, which has to be split into the sets F_3, F_4 and F_5. The contribution of the set F_3 is zero and the sets F_4 and F_5 will be treated separately.

4.4. Partition of TR3c

Diagram TR3c is very special as the orbits belonging to it can also be obtained as orbits from TR3a and/or TR3b when one of the t_i is equal to zero. Our job is to synchronize the partition

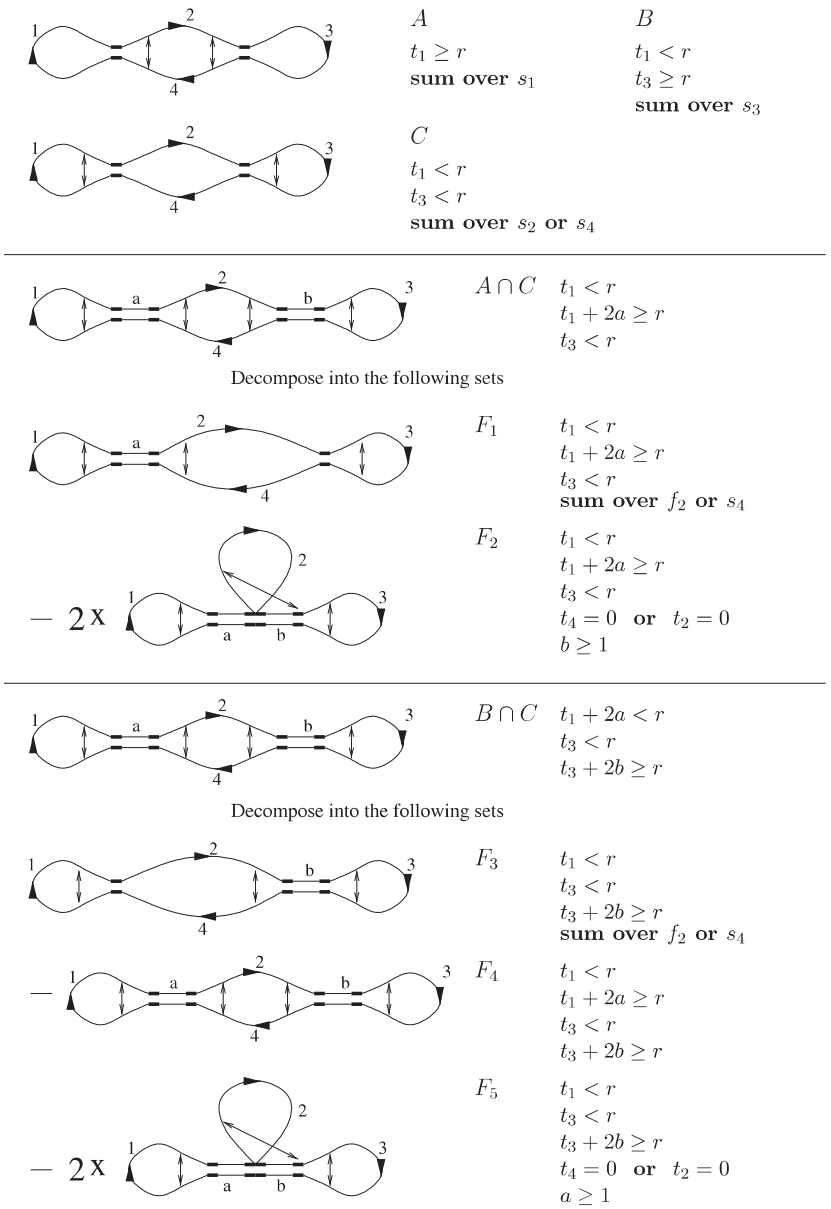

Figure 7. The TR3b diagram and its partition into three sets of orbits. The contribution of the orbits in each set can be easily shown to be zero. Below the line we sketch the intersection of the sets A and C, re-partitioned as F_1 minus F_2 and the sets B and C, re-partitioned as F_3 minus F_4 and F_5.

of TR3c with the partitions we chose for TR3a and TR3b. The relations between TR3c and the other diagrams are summarized in table 1.

An immediate consequence is that all TR3c orbits with $f_1 = f_2$ were already counted in TR3a: no set in TR3a has the restriction $s_2 \neq s_4$. Also *some* of the orbits from TR3c with $s_2 = f_3$ are counted in the sets A and C of TR3a. To understand precisely which orbits were counted, we notice that a TR3c orbit with $s_2 = f_3$ corresponds to a TR3a orbit with $s_1 = f_2$

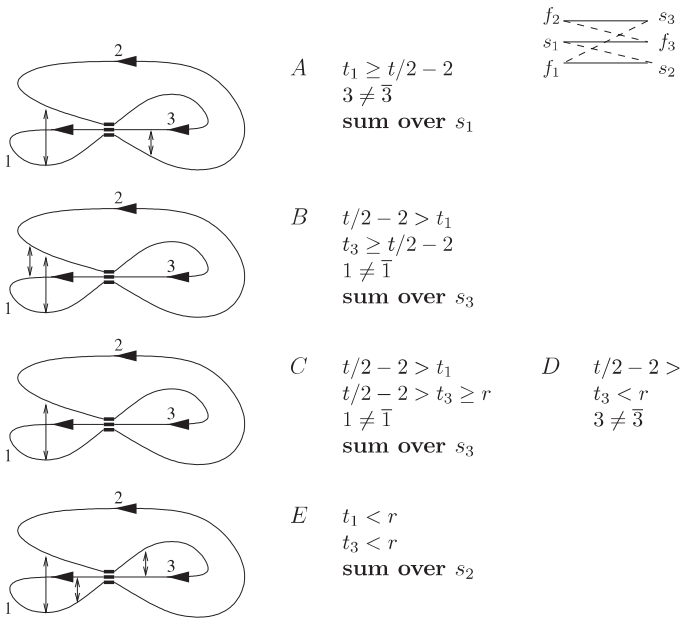

Figure 8. The TR3c diagram and its partition into five sets of orbits. In the upper right corner we illustrate the transitions through the intersection vertex undertaken by the original (full lines) and the partner (broken lines) orbits. The contribution of all sets except D can be easily shown to be zero. The set D is re-partitioned separately in figure 10.

Table 1. Summary of conversions between degenerate orbits of TR3c and two other diagrams. Here t_i denotes the length of the ith arc in diagram TR3c and t'_i denotes the same but for diagrams TR3a and TR3b; an 'R' denotes that the diagram is reversed. For example, the TR3c orbit with $f_1 = f_2$ can also be considered as a TR3a orbit with $s_2 = s_4$ and lengths of the arcs given by $t'_1 = t_1 - 1$, $t'_2 = 1$, $t'_3 = t_2 - 1$ and $t'_4 = t_3 + 1$.

TR3c	TR3a	Lengths			
$f_2 = f_1$	$s_2 = s_4$ ($t'_2 = 1$)	$t'_1 = t_1 - 1$,	$t'_2 = 1$,	$t'_3 = t_2 - 1$,	$t'_4 = t_3 + 1$
$s_2 = f_3$	$s_1 = f_2$ ($t'_2 = 1$)	$t'_1 = t_1 + 1$,	$t'_2 = 1$,	$t'_3 = t_2 - 1$,	$t'_4 = t_3 - 1$
$s_1 = f_2$	$s_3 = f_4$ ($t'_3 = 1$)	$t'_1 = t_1 - 1$,	$t'_2 = t_2 - 1$,	$t'_3 = 1$,	$t'_4 = t_3 + 1$
$s_2 = s_3$	$f_1 = f_3$ ($t'_3 = 1$)	$t'_1 = t_1 + 1$,	$t'_2 = t_2 - 1$,	$t'_3 = 1$,	$t'_4 = t_3 - 1$
$s_1 = f_2$ R	$s_1 = f_2$ ($t'_1 = 1$)	$t'_1 = 1$	$t'_2 = t_3 + 1$	$t'_3 = t_1 - 1$	$t'_4 = t_2 - 1$
$s_2 = s_3$ R	$f_1 = f_3$ ($t'_1 = 1$)	$t'_1 = 1$	$t'_2 = t_3 - 1$	$t'_3 = t_1 + 1$	$t'_4 = t_2 - 1$
$s_2 = f_3$ R	$s_3 = f_4$ ($t'_4 = 1$)	$t'_1 = t_2 - 1$	$t'_2 = t_3 - 1$	$t'_3 = t_1 + 1$	$t'_4 = 1$
$f_1 = f_2$ R	$s_2 = s_4$ ($t'_4 = 1$)	$t'_1 = t_2 - 1$	$t'_2 = t_3 + 1$	$t'_3 = t_1 - 1$	$t'_4 = 1$
TR3c	TR3b	Lengths			
$s_1 = f_1$	$s_2 = f_4$	$t'_1 = t_1 - 2$	$t'_2 = t_2 + 1$	$t'_3 = t_3$	$t'_4 = 1$
	$s_4 = f_2$	$t'_1 = t_3$	$t'_2 = 1$	$t'_3 = t_1 - 2$	$t'_4 = t_2 + 1$
$s_3 = f_3$	$s_4 = f_2$	$t'_1 = t_1$	$t'_2 = t_2 + 1$	$t'_3 = t_3 - 2$	$t'_4 = 1$
	$s_2 = f_4$	$t'_1 = t_3 - 2$	$t'_2 = 1$	$t'_3 = t_1$	$t'_4 = t_2 + 1$

and $t'_2 = 1$. Such an orbit can only belong to the set A, requiring $t'_1 + t'_2 \geqslant t/2$ and $t'_1 \geqslant t/4$, which is equivalent to $t_1 \geqslant t/2 - 2$ (see the 'Lengths' column of the table). The same applies to the reversed orbits from TR3c with $s_2 = f_3$ which were counted in TR3a set C. Thus orbits from TR3c with $t_1 \geqslant t/2 - 2$ must have the restriction $s_2 \neq f_3$ (the set A of figure 8). We also

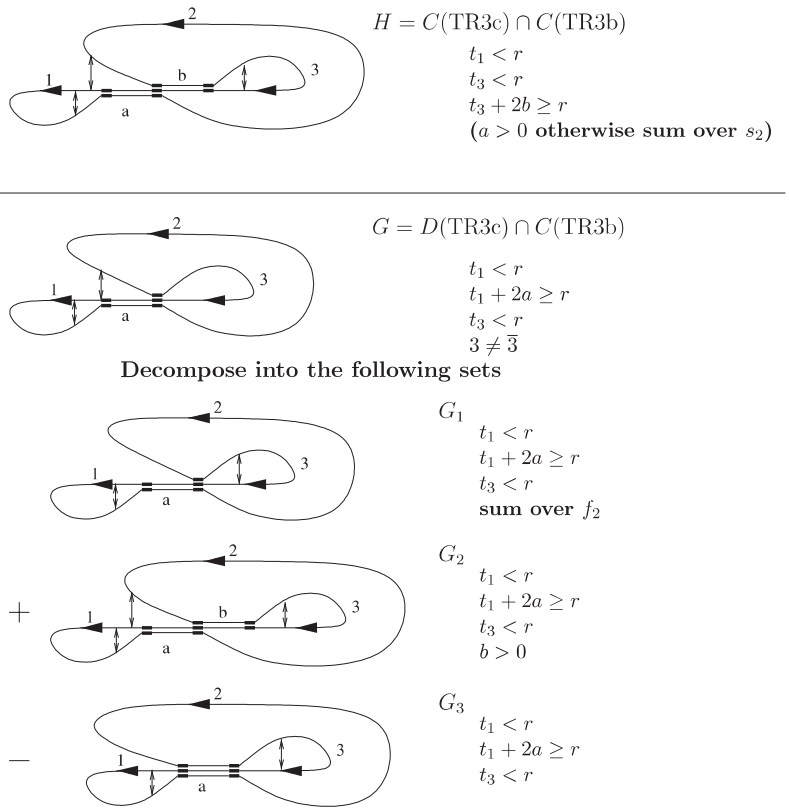

Figure 9. The set of orbits belonging to both set D of TR3c and set C of TR3b is re-partitioned as the set G_1 plus G_2 minus G_3. The contribution of the set G_1 is zero.

note that orbits from TR3c with $s_1 = f_2$ and $t_3 \geqslant t/2 - 2$ were already counted in TR3a sets B and D, warranting the use of the corresponding restriction for set B of figure 8.

The relation between TR3c and TR3b is simpler: if the lengths of an orbit from TR3c satisfy $t_1 < r$ and $t_3 < r$, then we must impose restrictions $s_1 \neq f_1$ and $s_3 \neq f_3$, which is reflected in the set E of figure 8.

Bringing the above information together we fix the partition of diagram TR3c, figure 8. All five partition sets are disjoint and the contributions of the sets A, B, C and E evaluate to zero by summing with respect to s_1, s_3 and s_3 and s_2 correspondingly. The set A is slightly special since, when $t_3 \geqslant t/2 - 2$, there is an additional restriction $s_1 \neq f_2$, but in this case one can sum over s_3 to obtain the zero result.

Despite the length restriction on the sets C and D, there are still orbits belonging to these sets and the set C of TR3b. These orbits are sketched in figure 9. When considering the intersection of C and TR3b, we assume $a > 0$ since, when $a = 0$, we can sum over s_2 to get zero. The contributions of this set will be evaluated separately.

The intersection of D and TR3b can be re-partitioned as G_1 plus G_2 minus G_3 with the set G_1 giving zero contribution (sum over f_2). We will show that the contributions of the sets G_2 and G_3 cancel each other exactly.

The last set to be decomposed is the set D of TR3c, see figure 10. Two dashed restrictions are denoting the situation when $s_3 = f_3$ and $s_2 = f_3$ cannot be satisfied *simultaneously*. Out of five partition sets, the sets D_1 and D_5 are immediately evaluated to zero, the contributions

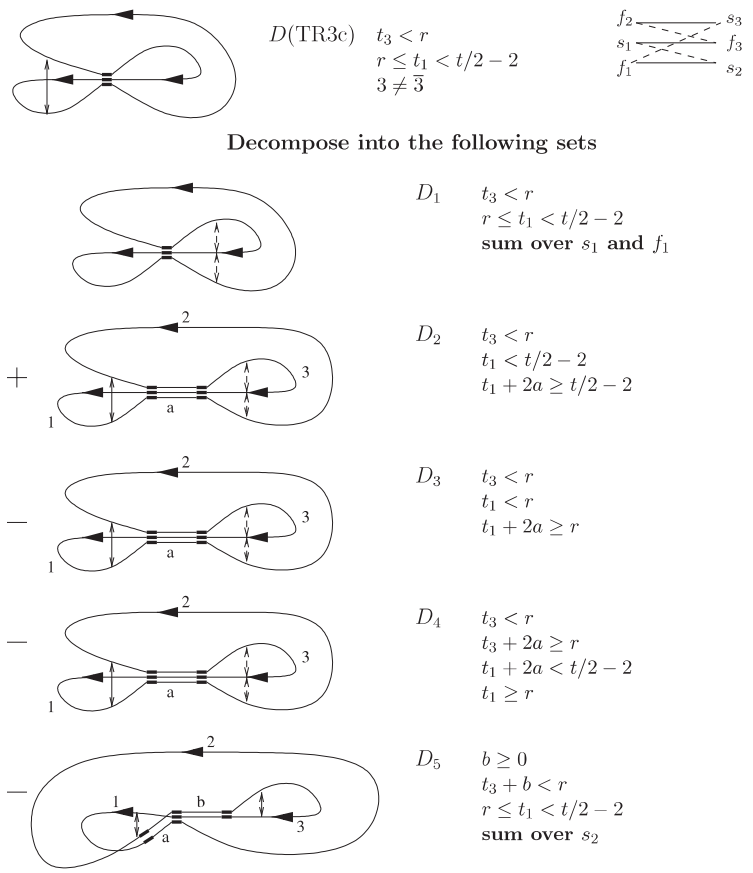

Figure 10. Re-partitioned set D of the TR3c diagram. Two broken restrictions denote the situation when $s_3 = f_3$ and $s_2 = f_3$ cannot be satisfied *simultaneously*. The sets D_1 and D_5 give zero contribution and the sets D_2 and D_3 produce contributions that cancel each other.

of the sets D_2 and D_3 clearly cancel each other, and thus only the contribution of the set D_4 survives.

4.5. Evaluating significant diagrams

If we denote the contribution of a set A by $|A|$, the total contribution to the τ^3 term of the form factor expansion takes the form

$$2(K_{\mathrm{TR3a}}(\tau) + K_{\mathrm{TR3b}}(\tau) + K_{\mathrm{TR3c}}(\tau)) = \frac{t^2}{B}(|F_2| + |F_4| + |F_5| - |E_2| + |E_3| - 2|H| - 2|D_4| - 2|G_2| + 2|G_3|). \quad (23)$$

The sign of each contribution is the sign displayed next to it on the corresponding diagram inverted if this diagram is from a two-way intersection of some sets (this is true for all sets but D_4). The overall factor of 2 is due to the TR symmetry and, in the case of the sets F and E, it is cancelled by the diagram symmetry factor of $1/2$, see figure 3.

When evaluating the contributions we use the following rules of thumb: (1) the length of the tangential intersections, denoted in the diagrams by letters a and/or b, can be set to 1 and

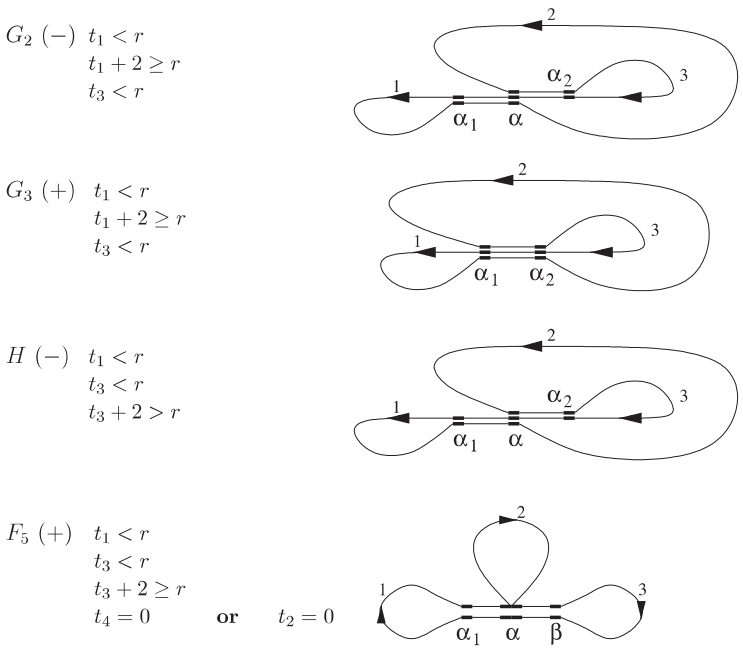

Figure 11. First four of the sets giving non-zero contributions.

(2) the restrictions can be ignored (see the appendix for a discussion of such approximations). We also notice that all orbits belonging to the above diagrams give a positive contribution (i.e. no more unitary factors left), which shows we are on the right track.

We begin by showing that the contributions of the sets G_2 and G_3 cancel each other. In figure 11 we introduced some extra notation necessary for the calculation. The contribution of the set G_2 can be written as

$$|G_2| = 2 \sum_{t_3<r} \sum_{\alpha_i} P^{t_1+1}_{(\alpha,\alpha_1)\to(\alpha_1,\alpha)} P^{t_2+1}_{(\alpha_1,\alpha)\to(\alpha,\alpha_2)} P^{t_3+1}_{(\alpha,\alpha_2)\to(\alpha_2,\alpha)} P^{1}_{(\alpha_2,\alpha)\to(\alpha,\alpha_1)}, \qquad (24)$$

where the summation is taken over αs such that there exist bonds (α, α_1) and (α, α_2) over the ranges of t_is outlined in the diagram. The two possible choices of t_1 are expressed as the factor of 2 and thus, due to the sum $t_1 + t_2 + t_3 + 4$ being fixed, the sum is essentially over $t_3 < r$. The arcs 1 and 2 are (relatively) long and therefore the corresponding transition probabilities can be approximated by their ergodic limit of $1/B$. We further sum over α_1 to obtain

$$|G_2| = \frac{2}{B^2} \sum_{t_3<r} \sum_{\alpha_i} P^{t_3+1}_{(\alpha,\alpha_2)\to(\alpha_2,\alpha)} P^{1}_{(\alpha_2,\alpha)\to(\alpha,\alpha_1)} = \frac{2}{B^2} \sum_{t_3<r} \sum_{\alpha,\alpha_2} P^{t_3+1}_{(\alpha,\alpha_2)\to(\alpha_2,\alpha)}. \qquad (25)$$

We evaluate the contribution of G_3 is a similar way:

$$\begin{aligned} |G_3| &= 2 \sum_{t_3<r} \sum_{\alpha_1,\alpha_2} P^{t_1+1}_{(\alpha_2,\alpha_1)\to(\alpha_1,\alpha_2)} P^{t_2+1}_{(\alpha_1,\alpha_2)\to(\alpha_1,\alpha_2)} P^{t_3+1}_{(\alpha_1,\alpha_2)\to(\alpha_2,\alpha_1)} \\ &= \frac{2}{B^2} \sum_{t_3<r} \sum_{\alpha_1,\alpha_2} P^{t_3+1}_{(\alpha_1,\alpha_2)\to(\alpha_2,\alpha_1)} \qquad (26) \end{aligned}$$

and notice that the final expressions for $|G_2|$ and $|G_3|$ are identical and thus cancel each other.

The sets H and F_5, figure 11, on the other hand, are identical themselves. The factor of 2 before the contribution of H is compensated by the factor of 2 in the diagram F_5 itself. Thus the total contribution $|F_5| - 2|H| = 0$.

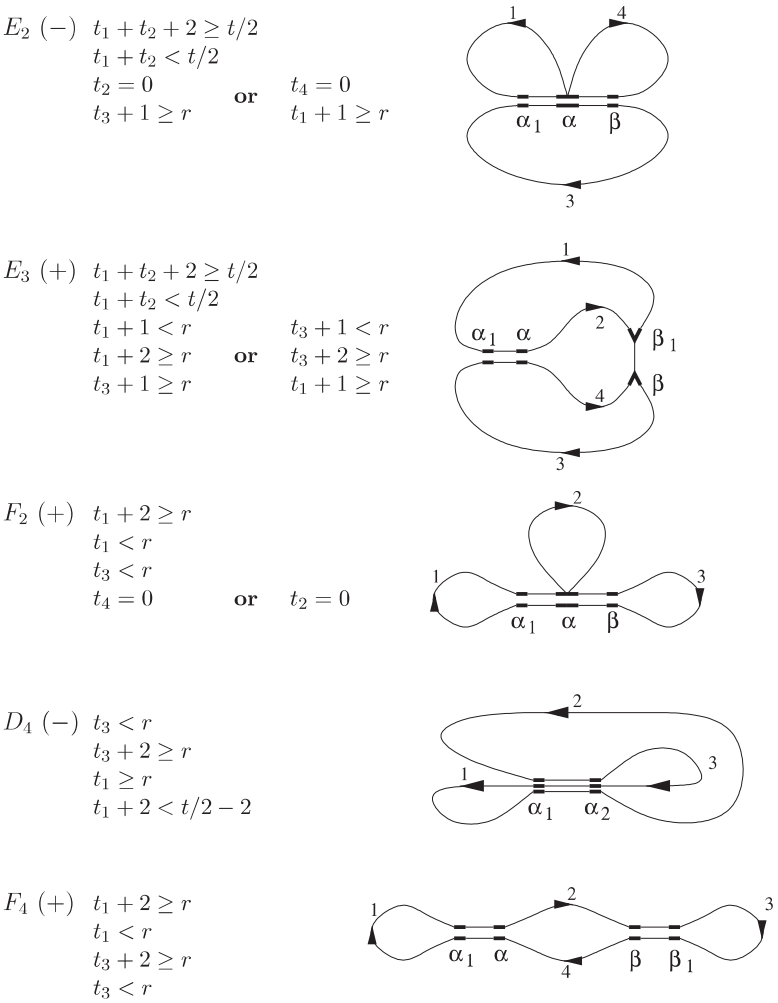

Figure 12. Sets E_2, E_3, F_2, D_4 and F_4 giving non-zero contributions. The diagram of E_2 was 'symmetrized' to highlight its similarity with F_2.

The contributions of the sets E_2, E_3 and F_2 are best grouped together. We start with E_3 (evaluating only one of the two cases and multiplying it by 2), figure 12. To simplify the notation when dealing with numbers of order t, such as $t/2$ and r, we ignore the constant corrections as they do not influence the limiting behaviour. The constraints imply $t_1 = r - 2$ and $t_1 + t_2 = t/2 \pm$ constant. Therefore the summation is over t_3 (or t_4). The summation is limited by the constraint $t_3 > r$ on the one side and by $t_3 < t - t_1 - t_2 \approx t/2$ on the other:

$$|E_3| = 4 \sum_{r<t_3<\frac{t}{2}} \sum_{\alpha,\alpha_1,\beta,\beta_1} P^{t_1+1}_{(\beta,\beta_1)\to(\alpha_1,\alpha)} P^{t_2+1}_{(\alpha_1,\alpha)\to(\beta_1,\beta)} P^{t_3+1}_{(\beta_1,\beta)\to(\alpha_1,\alpha)} P^{t_4+1}_{(\alpha_1,\alpha)\to(\beta,\beta_1)}$$

$$= \frac{4}{B^3} \sum_{r<t_3<\frac{t}{2}} \sum_{\alpha,\alpha_1,\beta,\beta_1} P^{t_4+1}_{(\alpha_1,\alpha)\to(\beta,\beta_1)} = \frac{4}{B^3} \sum_{r<t_3<\frac{t}{2}} \sum_{\alpha,\alpha_1} 1 = \frac{4}{B^2}\left(\frac{t}{2} - r\right), \tag{27}$$

where to perform the summation over all possible bonds (β, β_1) we invoke the probability conservation. The summation over all possible bonds (α, α_1) is just the number of bonds.

For E_2 the situation is very similar, but we choose to sum over t_4:

$$|E_2| = 4 \sum_{t_4 < \frac{t}{2} - r} \sum_{\alpha,\alpha_1,\beta} P^{t_1+1}_{(\beta,\alpha)\to(\alpha_1,\alpha)} P^{t_3+1}_{(\alpha,\beta)\to(\alpha_1,\alpha)} P^{t_4+1}_{(\alpha_1,\alpha)\to(\beta,\alpha)} P^{1}_{(\alpha_1,\alpha)\to(\alpha,\beta)}$$

$$= \frac{4}{B^2} \sum_{t_4 < \frac{t}{2} - r} \sum_{\alpha,\alpha_1,\beta} P^{t_4+1}_{(\alpha_1,\alpha)\to(\beta,\alpha)} P^{1}_{(\alpha_1,\alpha)\to(\alpha,\beta)}$$

$$= \frac{4}{B^2} \sum_{t_4 < \frac{t}{2} - r} \sum_{\alpha,\alpha_1} P^{t_4+2}_{(\alpha_1,\alpha)\to(\alpha,\alpha_1)}, \tag{28}$$

where, to get to the last line, we used the symmetry of the TR invariance, $P_{(\alpha_1,\alpha)\to(\alpha,\beta)} = P_{(\beta,\alpha)\to(\alpha,\alpha_1)}$, and the Markov property of the probabilities. Unfortunately, the contribution of E_2 depends on the particular structure of short orbits of the graph. Hopefully, the other contributions will help:

$$|F_2| = 4 \sum_{t_3 < r} \sum_{\alpha,\alpha_1,\beta} P^{t_1+1}_{(\alpha,\alpha_1)\to(\alpha_1,\alpha)} P^{t_2+1}_{(\alpha_1,\alpha)\to(\alpha,\beta)} P^{t_3+1}_{(\alpha,\beta)\to(\beta,\alpha)} P^{1}_{(\beta,\alpha)\to(\alpha,\alpha_1)}$$

$$= \frac{4}{B^2} \sum_{t_3 < r} \sum_{\alpha,\alpha_1,\beta} P^{t_3+1}_{(\alpha,\beta)\to(\beta,\alpha)} P^{1}_{(\beta,\alpha)\to(\alpha,\alpha_1)} = \frac{4}{B^2} \sum_{t_3 < r} \sum_{\alpha,\beta} P^{t_3+1}_{(\alpha,\beta)\to(\beta,\alpha)}, \tag{29}$$

where to get the final result we summed over α_1 and invoked the probability conservation. We notice that the sums in (29) and (28) are identical, up to a variable change, apart from the upper limit of the sum. Assuming, without loss of generality, that $r > \frac{t}{2} - r$, we obtain

$$|F_2| - |E_2| = \frac{4}{B^2} \sum_{\frac{t}{2} - r \leqslant t_3 < r} \sum_{\alpha,\beta} P^{t_3+1}_{(\alpha,\beta)\to(\beta,\alpha)}, \tag{30}$$

but now the sum is over large values of t_3. Thus

$$|F_2| - |E_2| = \frac{4}{B^3} \sum_{\frac{t}{2} - r \leqslant t_3 < r} \sum_{\alpha,\beta} 1 = \frac{4}{B^2} \left(r - \left(\frac{t}{2} - r \right) \right). \tag{31}$$

Bringing it together with $|E_3|$, we obtain

$$|F_2| - |E_2| + |E_3| = \frac{4r}{B^2}. \tag{32}$$

The next set to evaluate is D_4, figure 12. All arcs are long in this case, leading to the contribution

$$|D_4| = 2 \sum_{r \leqslant t_1 < \frac{t}{2}} \sum_{\alpha_1,\alpha_2} P^{t_1+1}_{(\alpha_2,\alpha_1)\to(\alpha_1,\alpha_2)} P^{t_2+1}_{(\alpha_1,\alpha_2)\to(\alpha_1,\alpha_2)} P^{t_3+1}_{(\alpha_1,\alpha_2)\to(\alpha_2,\alpha_1)}$$

$$= \frac{2}{B^3} \sum_{r \leqslant t_1 < \frac{t}{2}} \sum_{\alpha_1,\alpha_2} 1 = \frac{2}{B^2} \left(\frac{t}{2} - r \right). \tag{33}$$

In the final contribution, coming from the set F_4 of figure 12, the summation is over $t_2 + t_4 \approx t - 2r$. Arcs 1 and 3 are both long and of fixed length $r - 1$ or $r - 2$. This freedom of choice gives rise to the factor of 4 in front of the sum:

$$|F_4| = \frac{4}{B^2} \sum_{t_2+t_4=t-2r} \sum_{\alpha,\alpha_1,\beta,\beta_1} P^{t_2+1}_{(\alpha_1,\alpha)\to(\beta,\beta_1)} P^{t_4+1}_{(\beta_1,\beta)\to(\alpha,\alpha_1)}, \tag{34}$$

where the terms corresponding to arcs 1 and 3 have already being approximated by $1/B$. At least one of the arcs, 2 or 4, is long. Assuming, without loss of generality, that 2 is long, we have for the inner sum

$$\sum_{\alpha,\alpha_1,\beta,\beta_1} P^{t_2+1}_{(\alpha_1,\alpha)\to(\beta,\beta_1)} P^{t_4+1}_{(\beta_1,\beta)\to(\alpha,\alpha_1)} = \frac{1}{B} \sum_{\alpha,\alpha_1,\beta,\beta_1} P^{t_4+1}_{(\beta_1,\beta)\to(\alpha,\alpha_1)} = \frac{1}{B} \sum_{\beta,\beta_1} 1 = 1. \tag{35}$$

Thus the result for the set F_4 is

$$|F_4| = \frac{4}{B^2} \sum_{t_2+t_4=t-2r} 1 = \frac{4(t-r-r)}{B^2}. \tag{36}$$

The overall result is

$$\begin{aligned} 2(K_{\mathrm{TR3a}}(\tau) + K_{\mathrm{TR3b}}(\tau) + K_{\mathrm{TR3c}}(\tau)) &= \frac{t^2}{B}(|F_4| + |F_2| - |E_2| + |E_3| - 2|D_4|) \\ &= \frac{t^2}{B}\left(\frac{4}{B^2}(t-r-r) + \frac{4}{B^2}r - \frac{4}{B^2}\left(\frac{t}{2} - r\right)\right) = \frac{2t^3}{B^3} \to 2\tau^3. \end{aligned} \tag{37}$$

Taking into account that $K_{\mathrm{NTR3a}}(\tau) + K_{\mathrm{NTR3b}}(\tau) = 0$ [11], we obtain the final result $K_{\mathrm{TR3}}(\tau) = 2\tau^3$, QED.

5. Conclusions

The results of this paper complement those of [11] to form the derivation of the form factor of *generic* quantum graphs to third order.

While the derivation presented above is quite technical, the underlying idea is beautiful in its simplicity: the set of all orbits can be partitioned in such a way that the contribution of each partition set can be easily shown to be zero. This can be done without evaluating the contributions of individual orbits! The nonzero 'correct' result then arises from the intersections of the partition sets. The orbits in such intersections have generic properties: most of their arcs are long, making direct evaluation possible.

Here we presented one of the possible partitions and obtained the expected RMT result. The partition is based upon three basic diagrams, each being separately partitioned. It is very possible that there exists a 'unified' diagram with a simple partition. If such a diagram is found, it might make possible the derivation to all orders. Alas, it has so far evaded all attempts to find it.

The derivation is done for sequences of graphs satisfying two conditions: (a) graphs must be 'uniformly ergodic', as expressed by equation (8) and (b) the contribution of long self-retracing orbits must be negligible, equation (10). These conditions exclude such cases as Neumann star graphs, which are known to possess statistics different from RMT predictions. The families of graphs numerically found to satisfy the RMT hypothesis, such as Neumann complete graphs and Fourier star graphs, satisfy the above conditions.

Acknowledgments

The idea of the evaluation of the TR2 diagram, as it is done in section 4.1, was born in a discussion with Holger Schanz during the author's visit to Max-Planck-Institut, Göttingen, Germany. This idea later become the foundation for this entire work. The author is extremely grateful to Robert Whitney who proofread the paper, pointed out numerous mistakes and proposed simplifications. The paper was further improved following the extremely helpful remarks of the referee. A part of the research was performed while the author was working at the Weizmann Institute of Science, Rehovot, Israel, supported by the Israel Science Foundation, a Minerva grant, and the Minerva Center for Nonlinear Physics. This, and the encouragement provided by U Smilansky, is greatly appreciated.

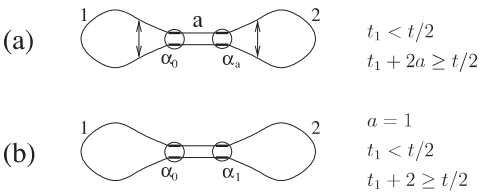

Figure A.1. In the first set, the tangential intersection must be of length $a > 0$. In the second set, the length of the intersection is not explicitly specified. It turns out that both sets contain exactly the same orbits.

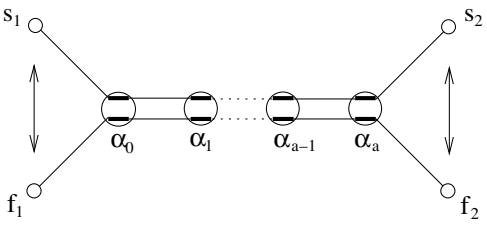

Figure A.2. Detailed view of the tangential intersection of length a, together with the adjacent vertices s_i and f_i.

Appendix. Setting $a = 1$ in the TR2 diagram

When we evaluated the contribution of the TR2 orbits, we dropped the constraints and set the length of the tangential intersection a to 1 (figure A.1). Here we discuss various aspects of this approximation.

For a given value of a, there are $2a$ choices of the length t_1 satisfying the inequalities of part (a) of figure A.1. For small a, the length of both arcs $(\alpha_0, s_1) \to (f_1, \alpha_0)$ and $(\alpha_a, s_2) \to (f_2, \alpha_a)$ are long and their contributions can be approximated by $1/B$. Thus the contribution of the TR2 diagram is

$$\frac{t^2}{B^3} \sum_{a=1}^{a'} 2a T_a, \tag{A.1}$$

where T_a is the contribution of the structure depicted in figure A.2, the tangential intersection of the length a. This contribution can be written as

$$T_a = \sum |\sigma_{s_1,\alpha_1}|^2 |\sigma_{f_1,\alpha_1}|^2 \prod_{k=0}^{a-2} |\sigma_{\alpha_k,\alpha_{k+2}}|^4 |\sigma_{s_2,\alpha_{a-2}}|^2 |\sigma_{f_2,\alpha_{a-2}}|^2 (1 - \delta_{s_1,f_1})(1 - \delta_{s_2,f_2}), \tag{A.2}$$

where the summation is taken over all indices s_i, f_i and α_k. Our aim is to show that the sum of $2aT_a$ is equal to the corresponding contribution from part (b) of figure A.1, given by $2\sum_{\alpha_0,\alpha_1} 1$. Opening up the brackets in (A.2) and performing a summation, where possible, over s_i and f_i, we get

$$T_a = \sum \prod_{k=0}^{a-2} |\sigma_{\alpha_k,\alpha_{k+2}}|^4 - \sum |\sigma_{s_1,\alpha_1}|^4 \prod_{k=0}^{a-2} |\sigma_{\alpha_k,\alpha_{k+2}}|^4 - \sum \prod_{k=0}^{a-2} |\sigma_{\alpha_k,\alpha_{k+2}}|^4 |\sigma_{s_2,\alpha_{a-2}}|^4 \tag{A.3}$$

$$+ \sum |\sigma_{s_1,\alpha_1}|^4 \prod_{k=0}^{a-2} |\sigma_{\alpha_k,\alpha_{k+2}}|^4 |\sigma_{s_2,\alpha_{a-2}}|^4 \tag{A.4}$$

$$= R_a - 2R_{a+1} + R_{a+2}, \tag{A.5}$$

where R_a is

$$R_a = \sum \prod_{k=0}^{a-2} |\sigma_{\alpha_k,\alpha_{k+2}}|^4. \tag{A.6}$$

The sum in (A.1) now folds to

$$\sum_{a=1}^{a'} 2aT_a = 2R_0 + 2a'R_{a'+2} - (2a'+2)R_{a'+1}. \tag{A.7}$$

Since R_0 is nothing other than $\sum_{\alpha_0,\alpha_1} 1$, to finish the proof we need to ensure that (i) the remainder of (A.7) is negligible and (ii) we can ignore orbits with $a > a'$. To this end we take a' to be of order t and refer to condition (10) which is obviously sufficient.

References

[1] Bohigas O, Giannoni M J and Schmit C 1984 *Phys. Rev. Lett.* **52** 1–4
[2] Haake F 2000 *Quantum Signatures of Chaos* (Berlin: Springer)
[3] Berry M V 1985 *Proc. R. Soc.* A **400** 229–51
[4] Sieber M and Richter K 2001 *Phys. Scr.* T **90** 128–33
[5] Sieber M 2002 *J. Phys. A: Math. Gen.* **35** L613–9 (*Preprint* nlin.CD/0209016)
[6] Mehta M L 1991 *Random Matrices* (New York: Academic)
[7] Gutzwiller M C 1971 *J. Math. Phys.* **12** 343–58
[8] Kottos T and Smilansky U 1997 *Phys. Rev. Lett.* **79** 4794–7
[9] Kottos T and Smilansky U 1999 *Ann. Phys.* **274** 76–124
[10] Berkolaiko G, Schanz H and Whitney R S 2002 *Phys. Rev. Lett.* **88** 104101
[11] Berkolaiko G, Schanz H and Whitney R S 2002 *Preprint* nlin.CD/0205014
[12] Barra F and Gaspard P 2000 *J. Stat. Phys.* **101** 283–319
[13] Grimmett G R and Stirzaker D R 1992 *Probability and Random Processes* (Oxford: Clarendon)
[14] Tanner G 2001 *J. Phys. A: Math. Gen.* **34** 8485–500
[15] Berkolaiko G and Keating J P 1999 *J. Phys. A: Math. Gen.* **32** 7827–41